arXiv:0907.0594v2 [hep-ph] 3 Sep 2010

# Efficient reconstruction of CMSSM parameters from LHC data – A case study

**Leszek Roszkowski**[a 1], **Roberto Ruiz de Austri**[b 2], and **Roberto Trotta**[c 3]

[a] *Department of Physics and Astronomy, University of Sheffield, Sheffield, S3 7RH, UK, and The Andrzej Soltan Institute for Nuclear Studies, Warsaw, Poland*

[b] *Instituto de Física Corpuscular, IFIC-UV/CSIC, Valencia, Spain*

[c] *Astrophysics Group, Imperial College, Blackett Laboratory, Prince Consort Road, London SW7 2AZ, UK*

**Abstract**

We present an efficient method of reconstructing the parameters of the Constrained MSSM from assumed future LHC data, applied both on their own right and in combination with the cosmological determination of the relic dark matter abundance. Focusing on the ATLAS SU3 benchmark point, we demonstrate that our simple Gaussian approximation can recover the values of its parameters remarkably well. We examine two popular non-informative priors and obtain very similar results, although when we use an informative, naturalness-motivated prior, we find some sizeable differences. We show that a further strong improvement in reconstructing the SU3 parameters can by achieved by applying additional information about the relic abundance at the level of WMAP accuracy, although the expected data from Planck will have only a very limited additional impact. Further external data may be required to break some remaining degeneracies. We argue that the method presented here is applicable to a wide class of low-energy effective supersymmetric models, as it does not require to deal with purely experimental issues, e.g., detector performance, and has the additional advantages of computational efficiency. Furthermore, our approach allows one to distinguish the effect of the model's internal structure and of the external data on the final parameters constraints.

[1] L.Roszkowski@sheffield.ac.uk
[2] rruiz@ific.uv.es
[3] r.trotta@imperial.ac.uk

# 1 Introduction

If softly broken low-energy supersymmetry (SUSY) provides a correct description of the particle physics realm at energy scales around a few hundred GeV and above, then superpartners are likely to be discovered at the LHC. One of the main goals of ATLAS and CMS experiments will be to identify those particles by determining their masses and other properties.

The actual outcome will depend not only on the LHC machine and detector performance but obviously also on the mass scales of the superpartners themselves. A whole plethora of different possibilities can be listed here, ranging from one extreme where all of the superpartners may come out to be too heavy to for the LHC reach, to another where all, or most, of them will be discovered. Unfortunately, basically the whole spectrum of options remains open even in perhaps the most economical SUSY framework, the Constrained Minimal Supersymmetric Model (Constrained MSSM, or CMSSM) [1] which includes the minimal supergravity (mSUGRA) model [2], as shown by a number of recent global fits of the CMSSM based on Bayesian statistics [3, 4] and on a $\chi^2$ approach [5, 6]. While the latter show a stronger preference for a fairly low SUSY mass scale, in the range of a few hundred GeV, the former point to a more cautious picture, where a much wider mass range remains allowed. This discrepancy is caused by the fact that, with the data that is currently available, even the CMSSM still remains to some extent underconstrained, and the specifics of the statistical and data analysis treatment can lead to fairly different results. It is therefore clear that selecting, or at least limiting, SUSY models by using LHC measurements is certainly going to be a very challenging task as there exist large degeneracies among the MSSM parameters that can lead to indistinguishable LHC signatures (see, e.g., Ref. [7]).

In preparation for dealing with real data, a number of approaches to particle mass reconstruction have been developed based on extracting kinematic information from one or more decay chains of superpartners, typically requiring two or more visible particles in the final state [8]. These and other techniques have been used by LHC experimental groups which have performed a large number of detailed studies in a few reference, or "benchmark", points, often selected in such a way as to typically allow several of the superpartners to be seen at the LHC.

In a recent extensive ATLAS Report [9], in the framework of the CMSSM/mSUGRA a so-called ATLAS SU3 benchmark point (which is specified below) was examined with Markov Chain Monte Carlo (MCMC) scans, with the aim of evaluating the expected accuracy of reconstructing CMSSM parameters: a common gaugino mass parameter $m_{1/2}$, a common scalar mass parameter $m_0$, a common trilinear term $A_0$, all evaluated at the unification scale $M_{\rm GUT} \simeq 2 \times 10^{16}$ GeV, plus a Higgs vacuum expectation values $\tan\beta$. Assuming an integrated luminosity of $1\,\mathrm{fb}^{-1}$, a dilepton and lepton+jets edge analysis of the decay chain $\widetilde{q}_L \to \chi_2^0(\to \widetilde{l}^{\pm} l^{\mp}) q \to \chi_1^0 l^+ l^- q$ and the high-$p_T$ and large missing energy analysis of the decay chain $\widetilde{q}_R \to \chi_1^0 q$ were performed, where $\widetilde{q}_L$ ($\widetilde{q}_R$) denotes the first or second generation left (right) squark, $\chi_{1,2}^0$ the first and second neutralino and $\widetilde{l}$ an intermediate slepton. It was concluded that $m_{1/2}$ and $m_0$ could be reconstructed with adequate accuracy, while prospects for $\tan\beta$ looked somewhat poorer, and even more so for $A_0$ (see Ref. [9], pp. 1617, ff).

In this paper we perform an independent analysis of the ATLAS SU3 point using the publicly available information about the expected ATLAS capabilities to measure the SU3 mass spectrum. We first demonstrate that a simple modelling of the mass spectrum constraints in an effective

likelihood is sufficient to reproduce with reasonable accuracy the results of the full ATLAS analysis, while being much more economical in terms of computational requirements, when we use the same linear, or flat (as defined below) prior. We then build on the ATLAS analysis by examining the impact of two other priors. We find that non-informative priors (i.e., priors whose characteristic scale is much larger than the support of the likelihood) lead to approximate prior-independence in the posterior, thus significantly improving with respect to the current situation. On the other hand, if one imposes extra theoretical prejudice in the prior (by choosing a prior that penalizes fine-tuning), the posterior is still quite strongly affected.

We also compare with the limits that can be obtained using a maximum likelihood analysis, and we show that the choice of statistics (Bayesian or maximum likelihood) no longer matters once one combines ATLAS data with cosmological relic abundance determinations. We clarify what rôle is played by assuming a specific theoretical model (here the CMSSM) in complementing the information coming from the ATLAS measurements with model-specific theoretical correlations between masses of the observables.

In the second step, we go beyond the ATLAS analysis by applying additional information about the cosmological relic density $\Omega_\chi h^2$ of the lighest neutralino $\chi_1^0$ (below often denoted by $\chi$ for simplicity), assumed to be dark matter (DM) in the Universe. The dark matter abundance clearly provides additional information about the model at hand, and in this analysis we aim at obtaining a quantitative measure for the extra constraining power that it provides, on top of that expected from the ATLAS data. Here we first impose WMAP uncertainties on $\Omega_\chi h^2$ and demonstrate a significant improvement in the determination of the CMSSM parameters, especially $m_0$. Next we investigate the impact of further reducing the observational errors on $\Omega_\chi h^2$ to an accuracy as expected from Planck, and show that this will lead to only a further modest improvement. We also comment on the impact of some other commonly used constraints, in particular from $b \to s\gamma$ and $(g-2)_\mu$, which we, however, do not apply here. Finally, we examine the impact of the different constraints from ATLAS and cosmology on the uncertainties of mass measurements of several superpartners and on predictions for the scattering cross section relevant for direct detection of dark matter experiments.

The paper is organized as follows. In Sec. 2 we present a setup of our analysis for the ATLAS SU3 point in the CMSSM, including details of our scans of the CMSSM parameters. In Sec. 3 we present our numerical results for the posterior probability density functions (pdfs), including a discussion of an impact of adding further assumptions and information. In Sec. 4 we compare some of these with the alternative measure of the profile likelihood. We summarize our findings in Sec. 5.

## 2 Setup and benchmark point

### 2.1 The ATLAS SU3 benchmark point

We examine the ATLAS SU3 benchmark point for which input values of CMSSM parameters are given on the left side of Table 1. Since in the ATLAS analysis errors of relevant SM parameters ("nuisance parameters") were not included, we assume that the benchmark values for the nuisance parameters are set at their central values as given on the right side of Table 1. In the reconstruction done below, we then allow the nuisance parameters to vary and we constrain them using the likelihood given below.

| CMSSM parameter | ATLAS SU3 benchmark value | SM parameter | Input value |
|---|---|---|---|
| $m_{1/2}$ | 300 GeV | $M_t$ | 172.6 GeV |
| $m_0$ | 100 GeV | $m_b(m_b)^{\overline{MS}}$ | 4.20 GeV |
| $\tan\beta$ | 6.0 | $\alpha_s(M_Z)^{\overline{MS}}$ | 0.1176 |
| $A_0$ | $-300$ GeV | $1/\alpha_{\rm em}(M_Z)^{\overline{MS}}$ | 127.955 |
| $\mathrm{sgn}(\mu)$ | $+$ | | |

Table 1: Left side: input CMSSM parameters values for the ATLAS SU3 benchmark point. Right side: input values of relevant SM parameters used in the numerical analysis.

| superpartner | mass | superpartner | mass | superpartner | mass |
|---|---|---|---|---|---|
| $\chi_1^0 (= \chi)$ | 117.9 GeV | $\widetilde{e}_L$, $\widetilde{\mu}_L$ | 230.8 GeV | $\widetilde{d}_L$ | 666.2 GeV |
| $\chi_2^0$ | 223.4 GeV | $\widetilde{e}_R$, $\widetilde{\mu}_R$ | 157.5 GeV | $\widetilde{d}_R$ | 639.0 GeV |
| $\chi_3^0$ | 463.8 GeV | $\widetilde{\nu}_e$, $\widetilde{\nu}_\mu$ | 217.5 GeV | $\widetilde{u}_L$ | 660.3 GeV |
| $\chi_4^0$ | 479.9 GeV | $\widetilde{\tau}_1$ | 152.2 GeV | $\widetilde{u}_R$ | 644.3 GeV |
| $\chi_1^+$ | 224.4 GeV | $\widetilde{\tau}_2$ | 232.4 GeV | $\widetilde{b}_1$ | 599.0 GeV |
| $\chi_2^+$ | 476.4 GeV | $\widetilde{\nu}_\tau$ | 216.9 GeV | $\widetilde{b}_2$ | 636.6 GeV |
| $\widetilde{g}$ | 717.5 GeV | | | $\widetilde{t}_1$ | 446.9 GeV |
| | | | | $\widetilde{t}_2$ | 670.9 GeV |

Table 2: Superpartner mass spectrum for the ATLAS SU3 point.

Since LHC data is rather unlikely to differentiate among the flavors of the squarks of the first two generation, in what follows we denote them all by a common symbol $\widetilde{q}$, and by $m_{\widetilde{q}}$ their average mass, similarly as in Ref. [9]. On the other hand, $\widetilde{l}$ will denote the lightest slepton and $m_{\widetilde{l}}$ its mass. In the case of the ATLAS SU3 point its rôle is played by $\widetilde{\tau}_1$.

The resulting mass spectrum, as computed using the SoftSusy code version 1.0.18 [10] in the 1-loop approximation is given in Table 2. By comparing with the mass spectrum for the ATLAS SU3 point given in Ref. [9] (cf. Table 2 on page 1516), we can see some differences, especially a systematic shift in squark masses by a few tens of GeV, which may be due to using different numerical codes, approximations (although in both cases 1 loop expressions are applied) as well as different inputs in SM parameter values. While this will contribute to some differencies we will find with the ATLAS results, at the end these discrepancies are of secondary importance, as we discuss below.

### 2.2 The likelihood function

The study performed by the ATLAS Collaboration on the SU3 point reports the expected accuracy in the reconstruction of some of the masses and mass differences in the benchmark SUSY spectrum given in Table 2. Dilepton edges will constrain $m_{\chi_1^0}$, $m_{\chi_2^0}$, $m_{\widetilde{q}}$ and $m_{\widetilde{l}}$ with fairly poor accuracy, while providing much tighter limits on the mass differences between the three latter quantities and the lightest neutralino, since these follow more directly from endpoint measurements. The endpoint in the dilepton invariant mass distribution is determined by the masses of the particles involved.

In the case of the SU3 point considered here, the two-body decay channel $\chi_2^0 \to \widetilde{l}^{\pm} l^{\mp}$ dominates, since $m_{\chi_2^0} > m_{\widetilde{l}}$, and the distribution of the invariant mass of the two leptons is triangular, with an endpoint given by [9] (p. 1619)

$$m^{\rm edge} = m_{\chi_2^0} \sqrt{1 - \left(\frac{m_{\widetilde{l}}}{m_{\chi_2^0}}\right)^2} \sqrt{1 - \left(\frac{m_{\chi_1^0}}{m_{\widetilde{l}}}\right)^2}. \tag{1}$$

A measurement of the dilepton endpoint leads to a relationship between $\chi_2^0$, $\chi_1^0$ and the slepton involved. Further mass distributions are considered in order to determine the masses of all the particles involved in the process, as described in Ref. [9] (pp. 1619, ff), along with event and cut selection procedures adopted in a reconstruction of the dilepton and other edges.

The observable quantities to be constrained by ATLAS are given by the set

$$\theta = \{m_{\chi_1^0}, m_{\chi_2^0} - m_{\chi_1^0}, m_{\widetilde{l}} - m_{\chi_1^0}, m_{\widetilde{q}} - m_{\chi_1^0}\}. \tag{2}$$

We further assume that the maximum likelihood (ML) value of $\theta$ obtained by ATLAS, $\theta_{\rm ML}$, corresponds to the value of the true benchmark point, $\theta_\star = \{117.9, 105.5, 34.3, 534.5\}$ GeV, where the numerical value is obtained from Table 2. In other words, we neglect realization noise, an assumption which is justified by the fact that $\langle \theta_{\rm ML} \rangle = \theta_\star$, where $\langle \cdot \rangle$ denotes an average over realizations. The likelihood function from ATLAS is then modeled as a Gaussian centered around the true value of the observable quantities,

$$-2 \ln \mathcal{L}_{\rm ATLAS} = \chi^2_{\rm ATLAS} = (\theta - \theta_{\rm ML})^t C^{-1} (\theta - \theta_{\rm ML}), \tag{3}$$

where the covariance matrix $C$ is given in Table 3 (and we have dropped an irrelevant normalization constant). It represents the full covariance between the masses and the mass differences. The covariance matrix includes statistical errors only; systematic errors are negligible.

The form of the ATLAS likelihood function given in Eq. (3) is a simple Gaussian approximation to the actual likelihood function that one would obtain from a full analysis of simulated ATLAS data. The latter is, however, not available outside the Collaboration, and therefore our approximation represents the best that can be reasonably done given the information that is expected to be publicly available. There are two reasons why it might be interesting to consider an approximate ATLAS likelihood function at the level of the SUSY mass spectrum. Firstly, it is not unreasonable that the simple approximation adopted here will give a fairly accurate representation of ATLAS capabilities (see below for further comments on how this compares with the full analysis carried out by the ATLAS Collaboration), and therefore provide a useful shortcut to quantitatively implementing the constraints that would result from a full analysis. Secondly, given the model-independent constraints on the low-energy SUSY mass spectrum, one can use them to constrain the high-energy parameters of any SUSY model of the MSSM class, in this case the CMSSM. As we shall show below, the constraining power included in the low-energy likelihood is then supplemented by the theoretical structure of the model itself.

We will now examine prospects for reconstructing the input values of the ATLAS SU3 point. We consider the following data combinations:

| | $m_{\chi_1^0}$ | $m_{\chi_2^0} - m_{\chi_1^0}$ | $m_{\tilde{l}} - m_{\chi_1^0}$ | $m_{\tilde{q}} - m_{\chi_1^0}$ |
|---|---|---|---|---|
| $m_{\chi_1^0}$ | $3.72 \times 10^3$ | 53.40 | $1.92 \times 10^3$ | $10.75 \times 10^2$ |
| $m_{\chi_2^0} - m_{\chi_1^0}$ | | 3.6 | 29.0 | $-1.3$ |
| $m_{\tilde{l}} - m_{\chi_1^0}$ | | | $1.12 \times 10^3$ | 4.65 |
| $m_{\tilde{q}} - m_{\chi_1^0}$ | | | | 14.1 |

Table 3: ATLAS covariance matrix employed in the analysis.

- ATLAS data only: including only the likelihood function given by Eq. (3);
- ATLAS data (as above) + WMAP-level uncertainty on dark matter abundance;
- ATLAS data (as above) + Planck-level uncertainty on dark matter abundance.

When including information about the cosmological dark matter abundance, we have to address the fact that the value of the neutralino relic abundance (computed using the code Micromegas [11]) for the ATLAS SU3 benchmark point, is $\Omega_\chi h^2 = 0.2332$, which is a factor of some 2.5 above the WMAP range of $0.1099 \pm 0.0062$ for the cosmological dark matter [12]. However, assuming standard Big Bang cosmology and that the CMSSM is correct, we would expect that for the actual measured value of the CMSSM parameters, for which ATLAS and/or CMS measurements are made, $\Omega_\chi h^2$ would lie in the WMAP range. It is therefore not unreasonable to examine the impact of the extra piece of information, both in terms of its value and uncertainty, which is provided by the cosmological relic density of dark matter. Notice that we do not rely here on a potential ability to reconstruct $\Omega_\chi h^2$ from LHC data alone [13] (which, on the other hand, could provide an important cross-check of our cosmological input) but use it as external constraint. Therefore, since the ATLAS analysis has been carried out for the ATLAS SU3 point, with the specific values of the CMSSM parameters, we also adopt to keep this central value for the relic abundance. On the other hand, we don't expect any major change in the numerical results presented below if $\Omega_\chi h^2$ were actually close to the WMAP range.

In our analysis we implement the cosmological dark matter determination as follows. Firstly, we assume that the true value of the relic abundance corresponds to the value computed for the benchmark point, and that WMAP-level constraints correspond to a Gaussian likelihood centered around that value with standard deviation given by the current WMAP uncertainty, namely $\sigma_{\rm WMAP} = 6.2 \times 10^{-3}$:

$$-2 \ln \mathcal{L}_{\rm WMAP} = \chi^2_{\rm WMAP} = \frac{(\Omega_\chi h^2 - 0.2332)^2}{\sigma^2_{\rm WMAP}}. \tag{4}$$

The Planck satellite is expected to improve the WMAP accuracy on the relic abundance by a factor $\sim 10$ [14]. When including Planck-level constraints, we therefore adopt the same likelihood as above but with a smaller standard deviation, $\sigma_{\rm Planck} = 6.2 \times 10^{-4}$. Since for the "bulk region" to which the ATLAS SU3 point belongs the theoretical error in the relic abundance is estimated to be tiny [15] we neglect it here. In other cases it can be much larger, primarily due to the larger uncertainties in computing mass spectra; for example in the focus point region it would likely dominate and this would cloud the potential impact of the cosmological data.

In order to facilitate a comparison with the ATLAS study [9], in this analysis we do not apply

any other constraints, e.g., from LEP, rare processes in heavy quark physics ($b \to s\gamma$, etc) or the anomalous magnetic moment of the muon $(g-2)_\mu$, which are routinely used in global analyses of the CMSSM and other popular SUSY models. We have also checked that fixing the nuisance parameters or marginalising over them has a negligible impact on the results. Therefore we only present results with the nuisance SM parameters fully marginalised, even though in the ATLAS analysis the SM parameters were fixed at their central values.

### 2.3 Scanning the CMSSM parameters

With the aim of reconstructing the true values of the defining parameters for the ATLAS SU3 point, we explore the CMSSM parameter space with the help of the Nested Sampling (NS) scanning technique, as implemented in the MultiNest algorithm [16].

We consider two different non-informative priors, that is, priors which contain minimal assumptions about the values of the parameters:

- **flat prior:** flat in $m_{1/2}, m_0, A_0, \tan\beta$, with the ranges: 50 GeV $\leq m_{1/2}, m_0 \leq$ 500 GeV, $2 \leq \tan\beta \leq 62$ and $-4$ TeV $\leq A_0 \leq 4$ TeV.
- **log prior:** flat in $\log m_{1/2}, \log m_0, A_0, \tan\beta$, with the same ranges: $\log(50) \leq \log m_0, \log m_{1/2} \leq \log(500)$ (in GeV), and as above for $A_0$ and $\tan\beta$.

Notice that we have employed here narrower ranges of $m_{1/2}$ and $m_0$ than the values of up to a few TeV used in our previous analyses [4, 18]. However, we have checked that enlarging the prior range to much larger values of $m_{1/2}, m_0$ (up to 4 TeV) has no impact on our reconstructed parameter values, as our algorithm correctly recovers the true parameter values even in the case of a much larger prior range. Finally, for the SM nuisance parameters we assume the same ranges as in our previous papers [4, 18]; in any case as we have mentioned above, the details of the treatment of nuisance parameters has basically no impact on the results presented here.

One of the aims of this work is to demonstrate that ATLAS data will achieve approximate prior-independence for the two choices of non-informative priors given above, which have been widely used in the literature so far and for which it has been shown that the current posterior for the CMSSM retains a fairly substantial prior dependence [18]. However, while this is encouraging, clearly that does not imply that one should expect the same to hold with any other choice of prior, of which there is an infinite range. Furthermore, in the Bayesian framework it is always possible to supplement the information contained in the likelihood by external prior information, for example by imposing "naturalness" constraints [20, 17]. In this case, one would not expect the posterior to remain independent of the prior, but actually to show stronger constraints than for the case of non-informative priors. In order to investigate to what extent a "naturalness" prior can supplement ATLAS data in constraining CMSSM parameters, we also consider an informative prior choice in section 3.4, with the following "CCR prior" (after Cabrera, Casas and Ruiz de Austri, who introduced it) [20],

- **CCR prior:** flat on $m_0, m_{1/2}, A_0, B$ but with an effective "penalty term" that naturally leads to low fine tuning among SUSY parameters.

The CMSSM is often treated as an effective theory following from mSUGRA which is parametrized in terms of the following parameters $\{m_0, m_{1/2}, A_0, B, \mu, \}$, which are then treated as in some sense

more fundamental. On the other hand, for the purpose of performing a numerical scaning of the model parameter space it is much more convenient to trade some of them for the CMSSM parameters which have a more direct phenomenological significance. (In addition one has the usual SM nuisance parameters.) In Refs. [20, 21] it has been shown that it is convenient to replace $\mu$ with $m_Z$, which is trivially integrated out. In addition, this procedure automatically takes into accounts the usual measure [22, 23] of the degree of fine-tuning. Furthermore, it is also convenient to trade the $B$ parameter for the derived quantity $\tan\beta$.

The change of variables $\{\mu, B\} \rightarrow m_Z, \tan\beta$ leads to the *effective prior* in the CMSSM variables

$$p_{\rm eff}(m_0, m_{1/2}, A_0, \tan\beta) \equiv J|_{\mu=\mu_Z}\; p(m_0, m_{1/2}, A_0, B, \mu = \mu_Z)\,, \tag{5}$$

where $p(m_0, m_{1/2}, A_0, B, \mu = \mu_Z)$ the prior for the mSUGRA parameters and $J$ is a Jacobian of the transformation, which is evaluated in the usual way from minimization equations of the Higgs scalar potential, $V(H_1, H_2)$. This way one arrives at an approximate form for the effective prior [20]

$$p_{\rm eff}(m_0, m_{1/2}, A_0, \tan\beta) \;\propto\; \frac{\tan^2\beta - 1}{\tan^2\beta(1+\tan^2\beta)}\frac{B_{\rm low}}{\mu_Z} p(m_0, m_{1/2}, A_0, B, \mu = \mu_Z)\;, \tag{6}$$

where $B_{\rm low}$ is the parameter $B$ evaluated at the electroweak scale and $\mu_Z$ is chosen so that it gives the correct of $m_Z$. The CCR prior is then defined as the effective prior $p_{\rm eff}(m_0, m_{1/2}, A_0, \tan\beta)$, Eq. (6), where we take a flat prior in $m_0, m_{1/2}, A_0, B$ and $\mu$.

# 3 Results

In this Section we present our numerical results from scans performed using the publicly available SuperBayes package version 1.35 [24], which we have modified in order to include a Gaussian likelihood from projected ATLAS data as described above.

## 3.1 Using ATLAS data only and non-informative priors

We begin by considering the constraining power on the CMSSM parameters of ATLAS mass spectrum data alone. In Figs. 1 and 2 we present 2-dimensional (2D) Bayesian posterior pdfs assuming the log and the flat prior, respectively, while the corresponding 1D pdfs for the log prior case are shown in Fig. 3. By examining the $(m_{1/2}, m_0)$ plane for the log prior in Fig. 1, we can see that both the 68% (inner regions) and the 95% (outer regions) total probability regions are well centered around the true value. Our algorithm recovers the best-fit point within the limits of numerical noise for all CMSSM parameters, except for $A_0$, where the reconstructed best-fit ends up in a wrong region of the parameter space due to a fundamental degeneracy discussed below. The posterior mean is also reasonably close to the true value (within $1\sigma$ for all parameters, except for $A_0$), although it is slightly skewed due to the asymmetric nature of the contours, which exhibit heavier tails than Gaussian (see also Fig. 3 below). On the other hand, $\tan\beta$ is somewhat less well reconstructed, yielding only an upper limit.

In contrast, $A_0$ is rather poorly constrained in this case, and actually shows a sign ambiguity. This is because it enters the analysis in a rather indirect way, mostly via the off-diagonal terms

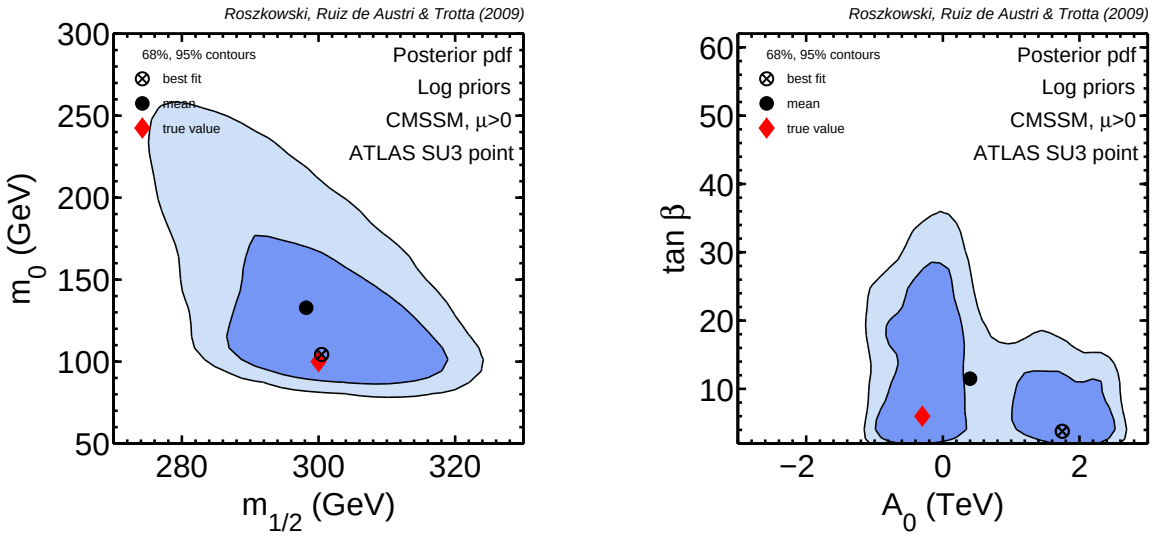



Figure 1: 2D posterior pdf for the case of applying ATLAS mass spectrum data alone, for some CMSSM parameter combinations and for the log prior choice. Compare with Fig. 12, p. 1638 of [9].

$X_\tau = A_\tau - \mu \tan\beta$ in the stau mass matrix, where $A_\tau$ is the value of $A_0$ at the EW scale evaluated with its RGE and $\mu$ is computed from the usual requirement of correct electroweak symmetry breaking. A closer examination reveals that, for $A_0 \sim 1$ TeV (in between the two $1\sigma$ regions in the right panel of Fig. 1), $X_\tau$ is minimized and the mass difference between $\widetilde{\tau}_2$ and $\widetilde{\tau}_1$ (which plays the rôle of the lightest slepton in the decay chain) goes to zero. Since in the ATLAS analysis only $\widetilde{\tau}_1$ was considered, such cases are not allowed. Our study thus reveals that in studying the decay $\chi_2^0 \to \widetilde{l}^{\pm} l^{\mp} \to \chi_1^0 l^+ l^-$ the exchange of both $\widetilde{\tau}_2$ and $\widetilde{\tau}_1$ should be considered, as for some values of $A_0$ their masses, and therefore also relative contributions, may be comparable.

In the case of the flat prior (Fig. 2) the emerging picture remains essentially identical, thus confirming that the prior choice becomes less of an issue once the constraining power of the data is sufficiently strong, as expected. Many of the features seen in Fig. 1 are displayed more clearly in Fig. 3 where the corresponding 1D pdfs are presented for the log prior case only; the flat prior produces very similar results and is therefore not shown. We give the 68% and 95% intervals of our reconstructed CMSSM parameters in Table 4. A comparison with the profile likelihood is carried out further below.

When considering posterior constraints on the SUSY mass spectrum, it is apparent that some of the constraints are much stronger than the likelihood function alone (which actually applies to a more general case of the MSSM) would seem to imply. For instance, the $1\sigma$ error on $m_{\chi_1^0}$ from the ATLAS likelihood is 60 GeV (cf. Table 3, where the likelihood $1\sigma$ range is obtained as the square root of the diagonal elements). However, the reconstructed neutralino mass within

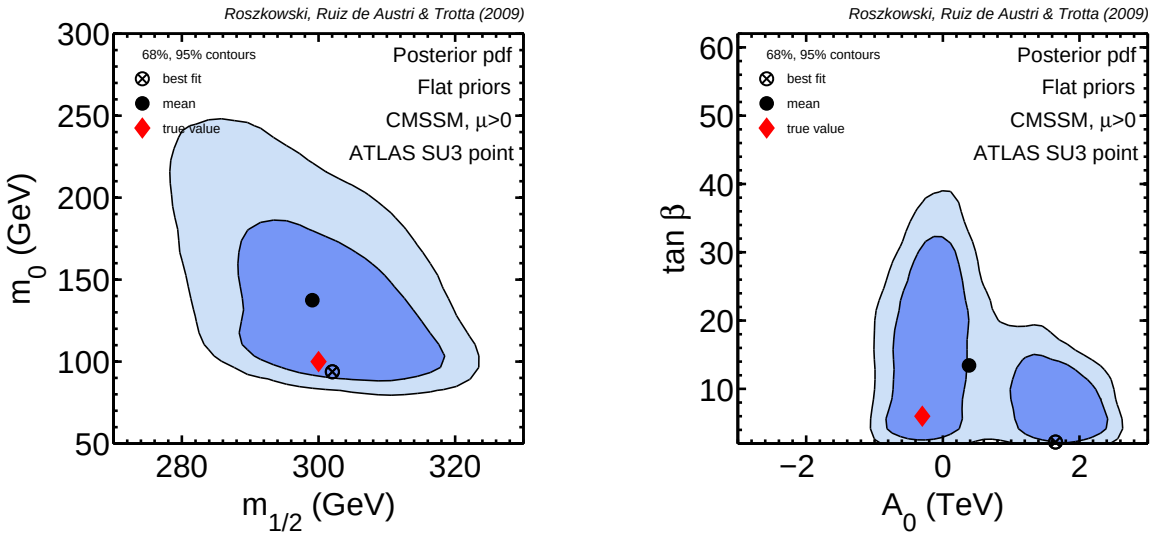



Figure 2: The same as in Fig. 1 but for the flat prior case. Notice that the two choices of priors lead to statistically indistinguishable results.

the CMSSM shows a much smaller error, of order $\sim 4$ GeV, cf. Table 4. The reason for this is that the information supplied by the likelihood is supplemented by the internal structure of the CMSSM parameter space, within which the masses of many of the sparticles are highly correlated. This is demonstrated in Fig. 4, where one can see that the correlation between masses in the spectrum within the CMSSM is nearly orthogonal to the constraints provided by ATLAS for the mass spectrum observables plotted in the Figures. One can think of this correlation as an additional *a priori* piece of information contained in the model. In other words, given the theoretical structure of the CMSSM, certain mass combinations in the spectrum (which are otherwise allowed by the projected ATLAS constraints, red ellipses in Fig. 4) are simply not allowed by the structure of the model. Therefore the final constraints on the spectrum are much tighter than the likelihood alone would imply. Supplementing the mass spectrum constraints with a model-specific implementation, as done here, has the additional advantage of displaying which part of the constraining power comes from the experimental data and which one from the theoretical properties of the model.

It is interesting to examine how well our procedure allows one to use the assumed ATLAS data alone to determine the relic abundance for the ATLAS SU3 point, in some analogy with what, for example, has been done for some other benchmark points in Refs. [13, 25]. This is shown in Fig. 5 where we find that, from the assumed ATLAS data alone one would obtain $\Omega_\chi h^2 = 0.253 \pm 0.034$, hence with a relative accuracy of $\sim 13\%$. For this specific point, this would imply that ATLAS data would determine the neutralino dark matter abundance at about $7\sigma$. Since the neutralino dark matter abundance for the ATLAS SU3 benchmark point is some 2.5 times larger than the value

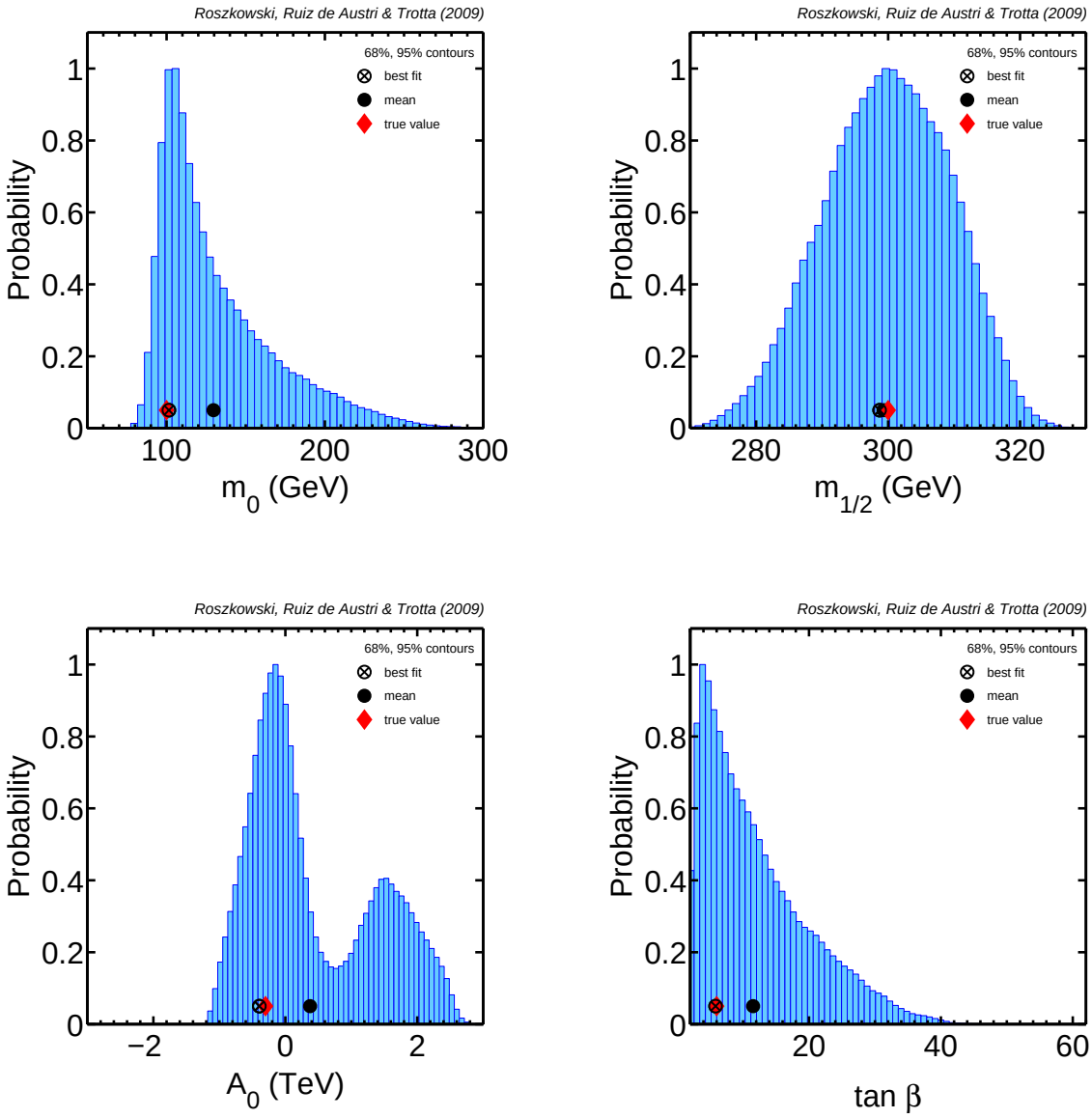



Figure 3: 1D posteriod pdf for the case of applying only ATLAS mass spectrum data, summarized in 1D projections. We show only the log prior case, for the flat prior case is essentially identical. It is clear that ATLAS data alone is not sufficient to reconstruct all of the CMSSM parameters. In particular, while $m_{1/2}$ is well measured, $A_0$ and $\tan\beta$ remain largely undetermined.

| Applying ATLAS data only | | | |
|---|---|---|---|
| Parameter | True value | Best fit | 68% (95%) range |
| $m_{1/2}$ (GeV) | 300 | 300.4 | $[288.2, 308.4]$, $([278.2, 316.3])$ |
| $m_0$ (GeV) | 100 | 104.3 | $[98.7, 173.6]$, $([89.8, 235.2])$ |
| $\tan\beta$ | 6.0 | 3.8 | $< 13.8$ ($< 27.4$) (1 tail) |
| $A_0$ (GeV) | -300 | 1749.7 | $[-568.3, 1701.8]$, $([-995.1, 2311.6])$ |
| $m_{\chi_1^0}$ (GeV) | 117.9 | 116.9 | $[113.7, 120.8]$, $([110.6, 123.7])$ |
| $\Omega_\chi h^2$ | 0.2332 | 0.2330 | $[0.2264, 0.2870]$, $([0.2096, 0.3450])$ |
| $\log\sigma_p^{SI}$ (pb) | -8.92 | -8.87 | $[-9.14, -8.42]$, $([-9.45, -8.04])$ |
| Applying ATLAS+WMAP-like data | | | |
| Parameter | True value | Best fit | 68% (95%) range |
| $m_{1/2}$ (GeV) | 300 | 302.3 | $[293.2, 310.7]$, $([285.5, 317.5])$ |
| $m_0$ (GeV) | 100 | 98.3 | $[95.9, 112.2]$, $([90.9, 151.6])$ |
| $\tan\beta$ | 6.0 | 5.5 | $< 7.3$ ($< 16.3$) (1 tail) |
| $A_0$ (GeV) | -300 | -228.2 | $[-498.1, 1437.6]$, $([-887.7, 2199.1])$ |
| $m_{\chi_1^0}$ (GeV) | 117.9 | 118.6 | $[115.1, 121.3]$, $([112.2, 123.8])$ |
| $\Omega_\chi h^2$ | 0.2332 | 0.2333 | $[0.2281, 0.2397]$, $([0.2225, 0.2454])$ |
| $\log\sigma_p^{SI}$ (pb) | -8.92 | -8.85 | $[-9.07, -8.51]$, $([-9.36, -8.03])$ |
| Applying ATLAS+Planck-like data | | | |
| $m_{1/2}$ (GeV) | 300 | 300.5 | $[295.7, 311.1]$, $([289.0, 317.6])$ |
| $m_0$ (GeV) | 100 | 99.4 | $[95.3, 106.1]$, $([92.0, 115.6])$ |
| $\tan\beta$ | 6.0 | 6.1 | $< 4.3$ ($< 11.3$) (1 tail) |
| $A_0$ (GeV) | -300 | -257.4 | $[-397.5, 1378.7]$, $([-700.1, 2045.5])$ |
| $m_{\chi_1^0}$ (GeV) | 117.9 | 118.0 | $[115.9, 121.3]$, $([113.3, 123.8])$ |
| $\Omega_\chi h^2$ | 0.2332 | 0.2332 | $[0.2327, 0.2338]$, $([0.2322, 0.2345])$ |
| $\log\sigma_p^{SI}$ (pb) | -8.92 | -8.88 | $[-8.99, -8.56]$, $([-9.20, -8.31])$ |

Table 4: Reconstructed values and errors for the input CMSSM parameters and for some key observables. We also give the best fit from our scan. The 68% and 95% ranges are computed from the posterior pdf as shortest intervals around the mean. For definiteness, we have employed the log prior scan but the results from the flat prior case are essentially identical.

currently preferred by cosmological observations, if we assume that the accuracy for the benchmark point is representative for the accuracy that ATLAS will actually find around a point with the correct cosmological relic abundance of about 0.11, our estimate is that ATLAS data alone would be able to determine the DM relic abundance at the level of $\sim 3\sigma$. Finally, in our present analysis we have ignored any theoretical error in the DM abundance prediction. While for the ATLAS SU3 point, which falls into the bulk region, such an error is likely to be very small, in general it should be folded in when producing the posterior shown in Fig. 5.

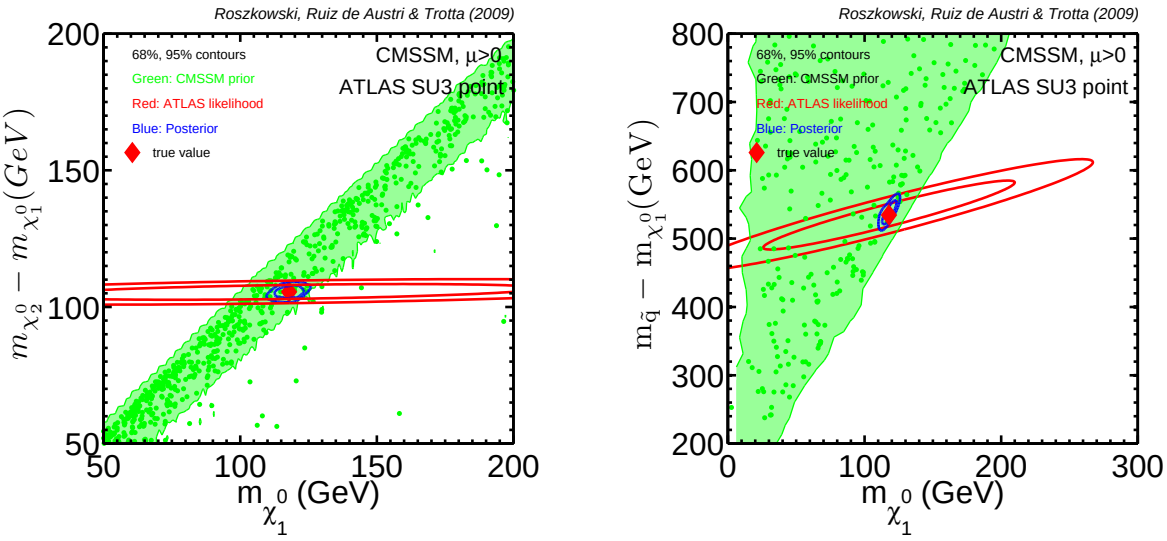



Figure 4: Illustration of the extra constraints coming from the assumption of the CMSSM as the theoretical framework. The parameter space accessible within the CMSSM is given by the green/light gray region (dots represents uniformly drawn samples), the red/dark gray (wide) ellipses are the ATLAS likelihood (as given by the covariance matrix of Table 3) while the blue/light gray (narrow) contours are the posterior constraints. In the context of the CMSSM this allows to derive much tighter constraints on $m_{\chi_1^0}$ than it would be possible based on the likelihood alone.

### 3.2 Comparison with the ATLAS Collaboration results

It is instructive to compare Figs. 1 and 2 with Fig. 12 in Section 9.3 of the ATLAS Report [9] where 2D marginal Bayesian posteriors are presented following the ATLAS MCMC analysis.[4] The overall shape of the high-probability $(m_{1/2}, m_0)$ and $(\tan\beta, A_0)$ regions is qualitatively similar although quantitatively we find somewhat less stringent bounds. In particular, we can see the largest difference in the case of $A_0$ where the highest probability region found in [9] lies on the boundary of the correct region found in our analysis, while the other, multi-TeV region, is in Ref. [9] absent altogether. There is also some difference in $m_0$ which in our case is not as well constrained as in Ref. [9].

It is however difficult to carry out a closer comparison, since not many details are given regarding the setup used in the ATLAS fitting analysis, in particular, about their treatment of SM nuisance parameters. Also, the ATLAS fitting analysis was performed directly from end-point measurements while we used a Gaussian approximation to the likelihood for masses and mass differencies alone,

[4] Although it is labeled "likelihood maps", the quantity plotted in Fig. 12 in of Ref. [9] is actually a marginal Bayesian posterior (Peter Wienemann - Private Communication), analogous to the one plotted in our Figs. 1 and 2.

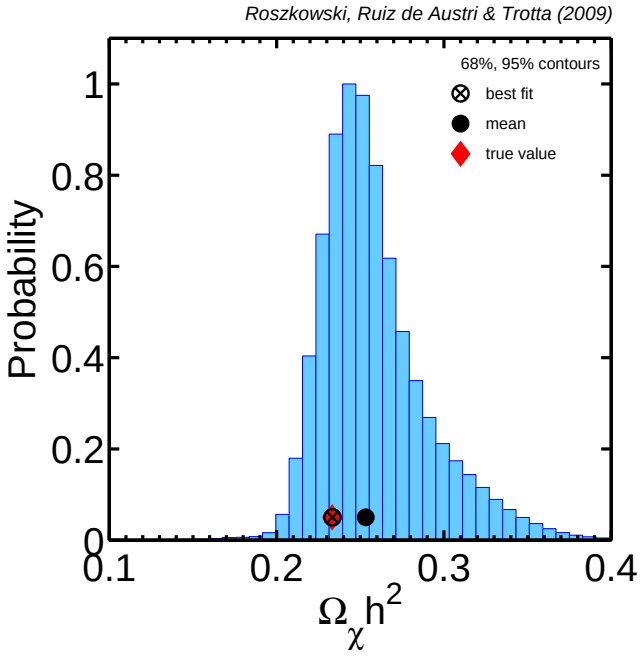



Figure 5: 1D posteriod pdf for the relic DM abundance $\Omega_\chi h^2$ of the neutralino, obtained from ATLAS data alone. We show only the log prior case, for the flat prior case is basically the same.

thus inevitably loosing a certain amount of information contained in the full analysis. It is, however, certainly encouraging that our "shortcut" method of reconstructing CMSSM parameters using a relatively crude Gaussian approximation to the full ATLAS analysis was able to recover quite compatible regions of SUSY parameters around their true values. The only exception is $A_0$, as explained above. As we show below, adding cosmological relic abundance constraints does help in further tightening some of the constraints. We conclude that, despite those differences, overall we find a reasonably good agreement with the ATLAS analysis. This suggests that not too much information is lost by carrying out the analysis employing an effective likelihood at mass spectrum level.

The advantage of our procedure is that it allows one to easily change the model-specific assumptions: if one replaces the CMSSM by another SUSY model that one is interested in, the analysis can be carried out without the need of going through the details of detector performance and obtaining the ATLAS likelihood numerically via Monte Carlo, thereby strongly reducing the computational requirements. In fact, our analysis requires about 24 hours on eight 3GHz processors, and it is therefore relatively computationally undemanding. Furthermore, it would be easy to adapt our method to employ a more complete likelihood function on the mass spectrum should this become available as part of the data products released by the LHC Collaborations. This would allow theo-

retical studies of the constraints implied on different SUSY models without the need to reproduce the full detector-specific signal reconstruction.

### 3.3 Impact of including the DM relic abundance

We now add to our likelihood function a constraint on the relic abundance uncertainties, as discussed in Sec. 2.2. In Fig. 6 we show the effect of imposing the ATLAS and WMAP data (ATLAS+WMAP) in the upper row, and an analogous case for the ATLAS+Planck case in the lower row. We plot the posterior for the log prior case; the flat prior case is basically identical. It is clear that, adding WMAP-like constraints improves the reconstructing power in determining the CMSSM parameters very considerably in the case of $m_0$ (and to some extent also $\tan\beta$), while the impact on the other two CMSSM parameters is fairly limited. This can be traced back to the fact that, in the bulk region, $\Omega_\chi h^2$ is determined primarily by the mass of the lightest slepton, via a $t$-channel exchange. Tightening the allowed range of $\Omega_\chi h^2$ selects a more peaked range of $m_{\widetilde{l}}$ and thus also $m_0$ on which it mostly depends. On the other hand, $m_{1/2}$, which primarily determines $m_\chi$, can be adequately constrained already by using only ATLAS data. As regards $A_0$, the bi-modality still remains as it is caused by the internal structure of the CMSSM. On the other hand, a further improvement of the error on $\Omega_\chi h^2$ to the level expected from Planck does not seem to improve the situation much beyond the ATLAS+WMAP case. In this context we again emphasize that, at this level of accuracy, it will be essential to achieve a similar, or better, level of theoretical errors, which may be challenging even for the bulk region.

In Fig. 7 we show the constraints on the masses of several superpartners obtainable with the three sets of data considered in this paper. We can see that in the case of the gauginos ($\chi^0_{1,2}$, $\chi^\pm_1$ and $\widetilde{g}$), whose masses are determined primarily by $m_{1/2}$ (which is well reconstructed), the errors are rather small, while for higgsino-like states ($\chi^0_{3,4}$ and $\chi^\pm_2$) the errors are large because of a poor determination of the $\mu$ parameter. For the states whose mass strongly depends on $m_0$ (spin-zero superpartners) the errors again reflect that of the common scalar mass, whose reconstruction, while reasonable, is not as good as for $m_{1/2}$.

The impact of further imposing other often used constraints from $b \to s\gamma$ and $(g-2)_\mu$ is in the present case rather limited. This is because the total error in the first quantity is still substantial while the dominant SUSY contribution to $(g-2)_\mu$ comes from sneutrino-chargino exchange. In the low mass region the masses of both particles are low and thus their contribution can be large enough to significantly reduce the discrepancy between the experimental data and the SM value.

Finally, we investigate how well one can predict the spin-independent cross section $\sigma_p^{SI}$ of dark matter neutralino scattering off a proton tested in direct detection experiments. As can be seen from Fig. 8, at 68% the value of $\sigma_p^{SI}$ will remain uncertain to within about one order of magnitude, while the neutralino mass will be very well constrained by LHC data as a reflection of the bounds on $m_{1/2}$. This is because in the case studied here $\sigma_p^{SI}$ is too a large extent determined by a $t$-channel heavy scalar Higgs exchange, where, in addition to $m_\chi$, the main two parameters are $\tan\beta$ and the Higgs mass which shows a considerable spread of values, mostly due to the larger uncertainty in $m_0$. Adding information about the DM relic abundance therefore improves the situation only in a fairly limited way.

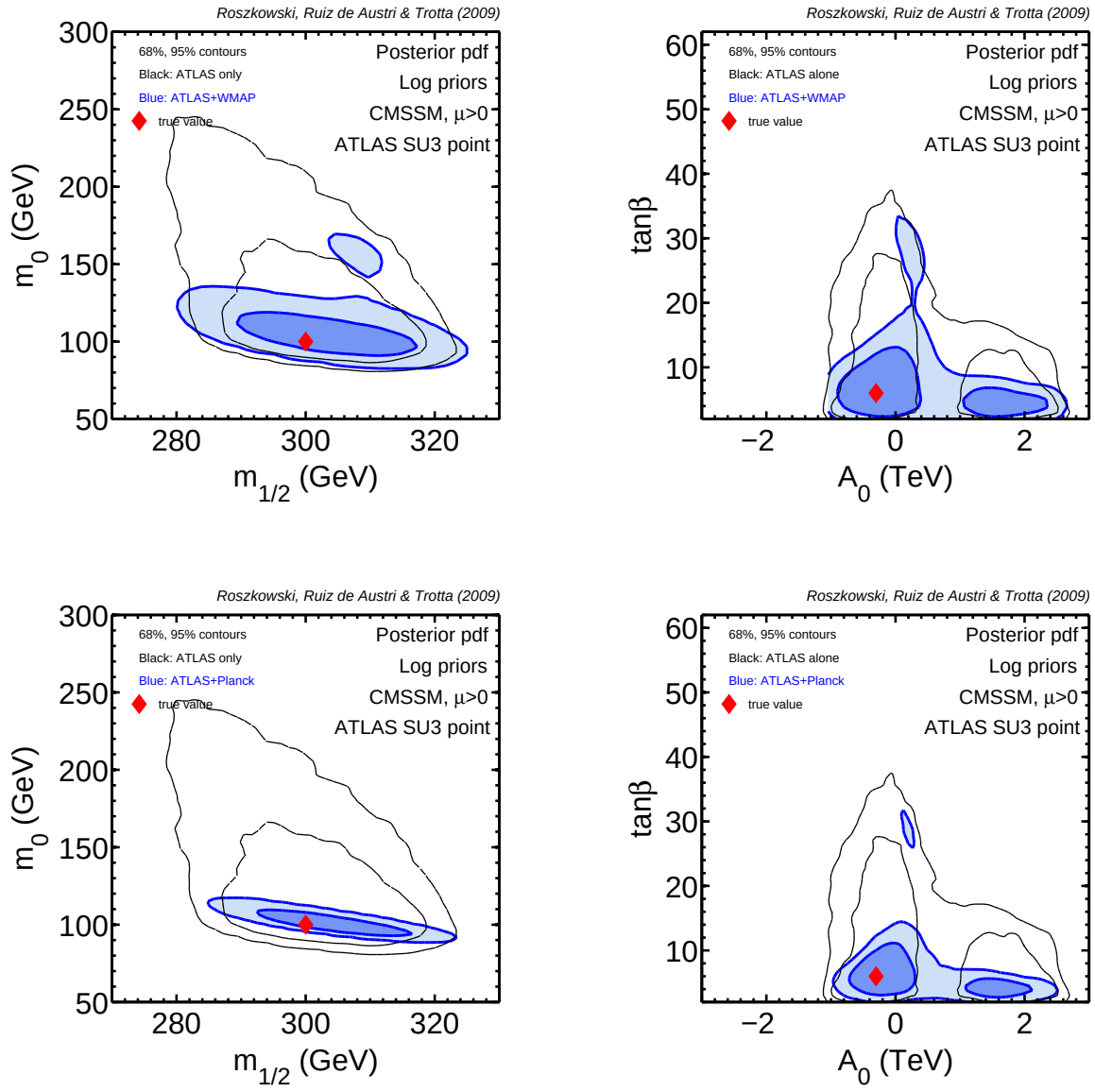



Figure 6: Impact of adding to the ATLAS data cosmological dark matter abundance determination with WMAP-like (upper row) and Planck-like (lower row) errors on $(m_{1/2}, m_0)$ (left panels) and $(\tan\beta, A_0)$ (right panels). Filled regions are for ATLAS plus either WMAP or Planck, while empty contours are for ATLAS only. Only the log prior case is presented; the flat one produces very similar results.

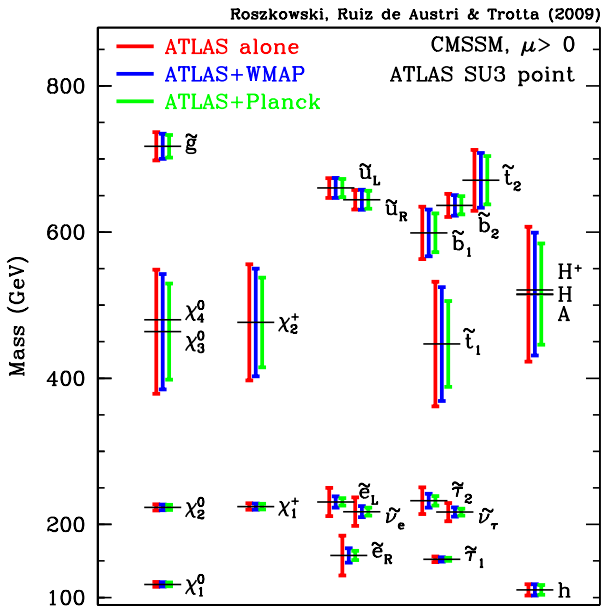



Figure 7: Reconstruction of the SUSY mass spectrum using projected ATLAS data only (red/leftmost errobar), adding WMAP-like constraints on the dark matter relic abundance (blue/central errorbar) and adding Planck-like dark matter constraints (green/rightmost errorbar). The errorbars represent the 68% range of the Bayesian posterior for the log prior. (The results for the flat prior is essentially identical.)

### 3.4 Impact of a naturalness prior

We now turn to investigating the impact that a highly informative prior choice based on naturalness considerations would have on the Bayesian posterior. The CCR effective prior implements Occam's razor penalization of regions of the parameter space exhibiting large fine-tunings [20]. This implies that the statistical weight of regions with large $\tan\beta$ is reduced, since fine-tuning generally increases with increasing $\tan\beta$. The same applies to the soft-terms, except for $m_0$ where lower fine-tuning is actually achieved in the TeV range, in the so-called hyperbolic branch/focus point (FP) region [26, 27].

The posterior pdf for the CCR prior for the CMSSM parameters is shown in Fig. 9 as blue-shaded 68% (darker) and 95% (lighter) regions, where for comparison we also show the non-informative log prior case (the corresponding black contours). We observe that the CCR prior leads to much tighter errors on especially $\tan\beta$, and to some extent also $m_0$, by assigning a larger penalty, and therefore stronger constraints, to "less natural" ranges of those parameters. The posteriors for $m_{1/2}$ and $A_0$, on the other hand, are only midly affected by the CCR prior. This is an example of how supplementing the information from the likelihood with a naturalness prior coming from theoretical prejudice leads to a posterior which can be significantly different from one obtained using non-informative log (or flat) prior.

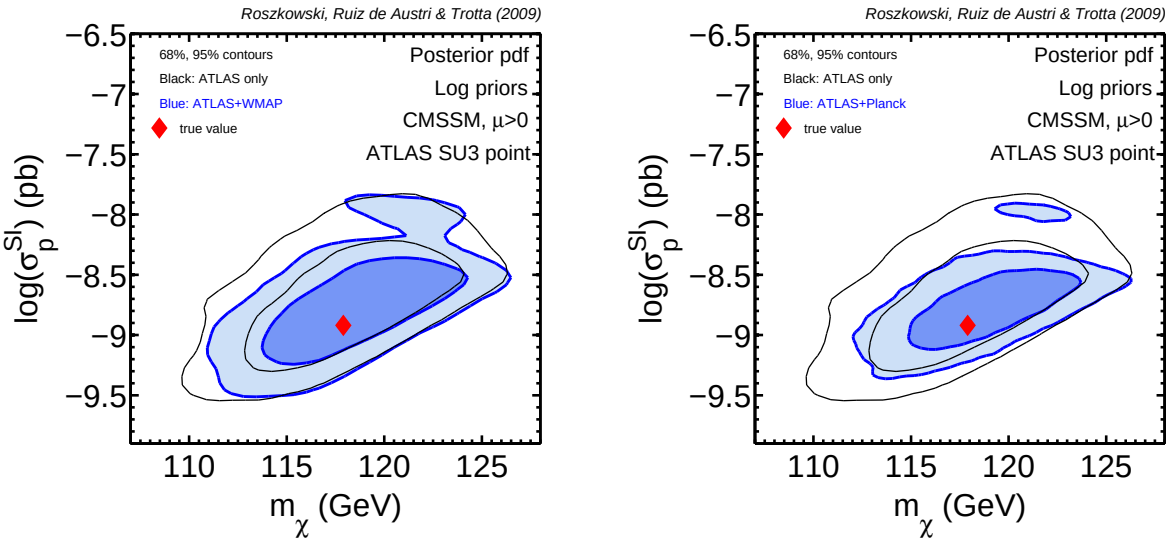



Figure 8: Impact of adding to the ATLAS data cosmological dark matter abundance determination with WMAP-like (left panel) and Planck-like (right panel) errors on the predictions for the spin-independent cross section of dark matter neutralino scattering off a proton, relevant for direct detection experiments. Filled regions are for ATLAS plus either WMAP or Planck, while empty contours are for ATLAS only.

## 4 Comparison with profile likelihood

In order to examine the robustness of the results obtained with the Bayesian posterior pdf, in this Section we compare them with what would be obtained by using a more traditional $\chi^2$-based analysis. We thus define the *profile likelihood* for, e.g., the CMSSM parameter $m_1$, where $m_1, \ldots, m_8$ comprise the 4 CMSSM parameters and the 4 SM nuisance parameters of Table 1, as

$$\mathfrak{L}(m_1) \equiv \max_{m_2,\ldots,m_8} \mathcal{L}(d|m), \tag{7}$$

where in our case $\mathcal{L}(d|m)$ is the full likelihood function. Thus in the profile likelihood one maximises the value of the likelihood along the other CMSSM and SM parameters, rather than integrating it out as in the marginal posterior. From the profile likelihood, confidence intervals are then obtained using the usual likelihood-ratio criterion. In the context of MCMC scans of the parameter space, the profile likelihood can be evaluated by simply finding the maximum likelihood value within a given bin. This has been studied before in the context of the CMSSM in Refs. [17, 18, 19]. Its interest lies in the fact that it is a prior independent measure. One should however be aware that, given current data, the numerical value of the profile likelihood remains dependent of the scanning algorithm employed, see the analysis in Ref. [19]. This problem is not relevant for the current paper, as we

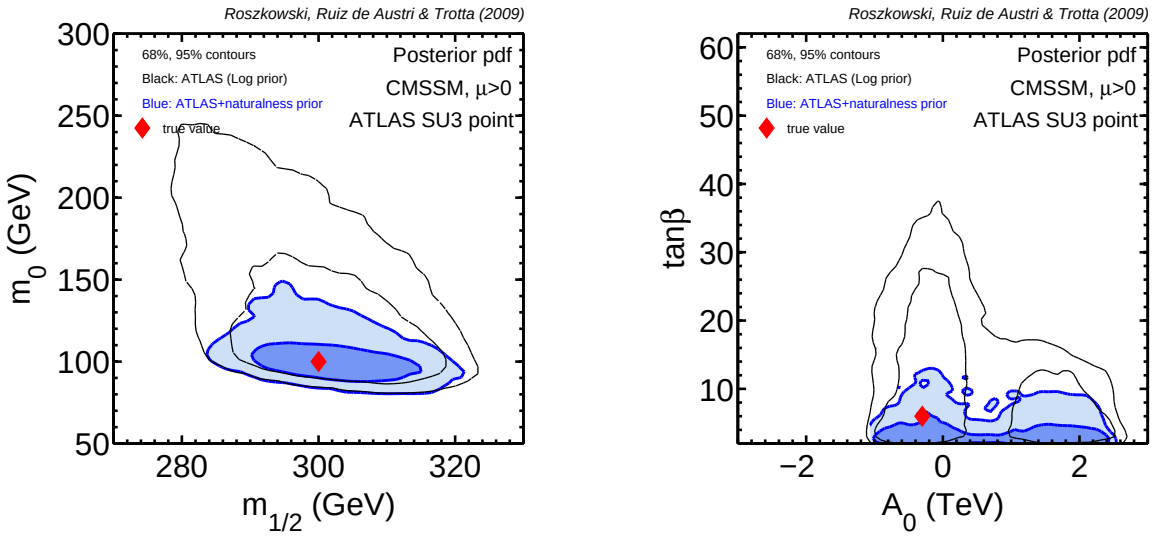



Figure 9: 2D posterior pdf for the case of applying ATLAS mass spectrum data alone with an informative naturalness prior (the CCR prior, filled contours), compared with the posterior obtained using non-informative log priors (empty contours).

are dealing with simulated data and we can thus double check that our profile likelihood correctly peaks near the true maximum likelihood value. Since we have found above little prior dependence of the posterior pdf, this suggests that the posterior pdf is dominated by the likelihood. Therefore we generically expect that the profile likelihood will give similar statistical results as the posterior studied above.

This is indeed confirmed in the top row of Fig. 10, where we present the 68% (inner contours) and the 95% confidence regions (outer contours) of the profile likelihood for the ATLAS-only data case and we compare them with the analogous regions derived from the posterior pdf presented earlier in Fig. 1. We show only the log prior case as the profile likelihood is prior independent (which we have verified numerically). We can see that at the 95% CL from the profile likelihood is quite similar to the corresponding 95% region derived from the Bayesian posterior for all parameters, except for $m_0$, for which the profile likelihood yields looser constraint. It is worth noticing that the posterior pdf yields a somewhat better reconstruction of $m_0$ and $\tan\beta$ and a similar one for the other CMSSM parameters. However, the relative merits of the reconstructed confidence regions from the posterior or from the profile likelihood cannot be assessed here. It is in general a difficult task to decide which statistics yields the "best" results (however one chooses to define this). A possible way forward would be to carry out a coverage study of the quoted confidence intervals, which is beyond the scope of this paper.

On the other hand, what is encouraging is that, when the data becomes sufficiently constraining,

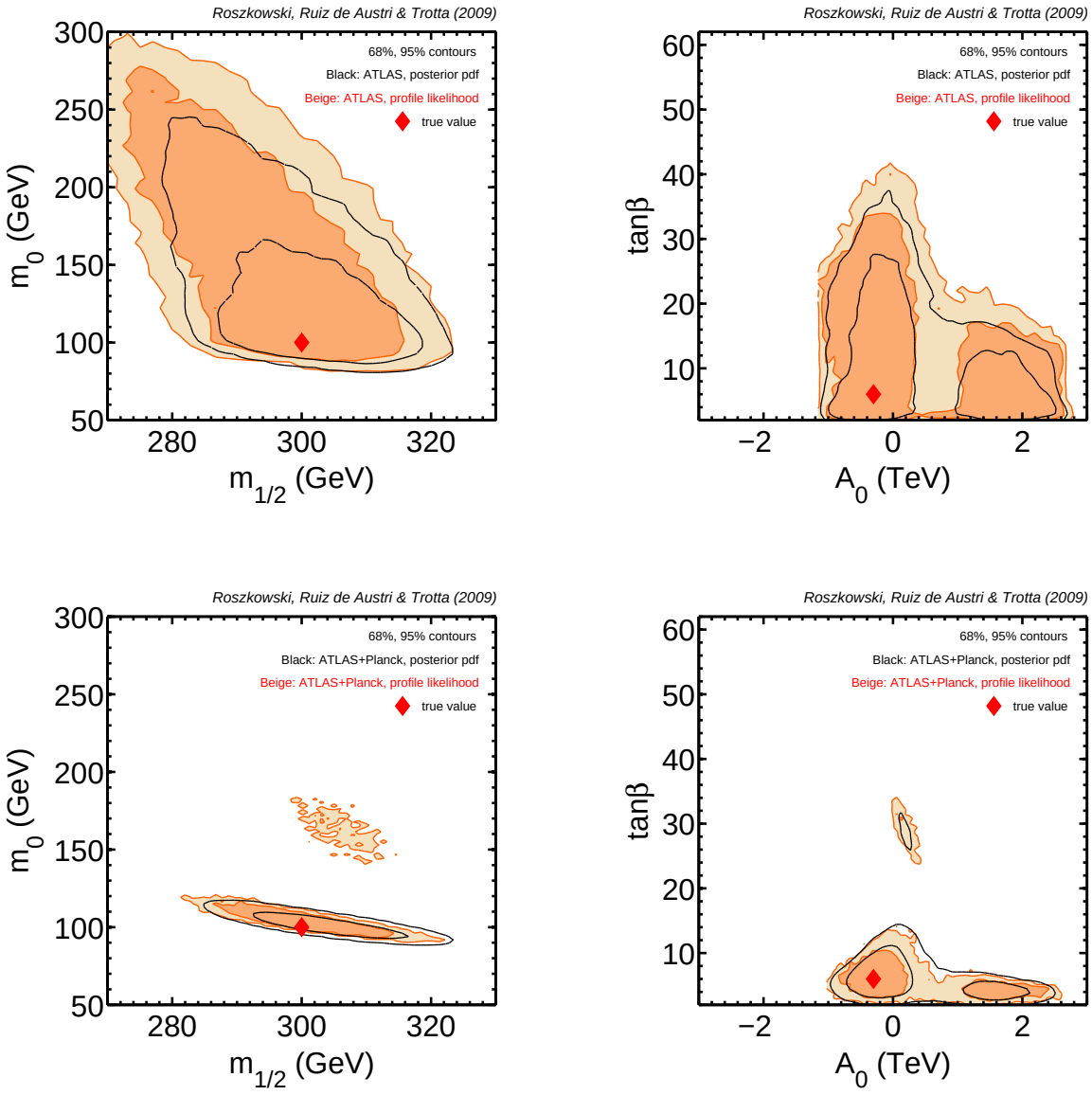



Figure 10: Comparison between the profile likelihood (filled) and posterior (empty contours) using ATLAS mass spectrum data only (top row) and adding Planck (bottom row). With this combination of data, the choice of statistics (Bayesian posterior or profile likelihood) becomes almost irrelevant, giving intervals that match at the 10% level.

both statistical quantities produce essentially equivalent confidence intervals. This is presented in

Fig. 10 for the ATLAS+Planck case, which should be compared with the bottom row of Fig. 6.

## 5 Summary and conclusions

In this paper we have examined prospects for reconstructing supersymmetric parameters from assumed future data that one can reasonably expect to become available. To this end we focused on the Constrained MSSM and on the benchmark point ATLAS SU3.

By following the ATLAS assumptions as closely as possible without having access to the full simulated likelihood function, we arrived at generally rather similar results for the reconstruction of the CMSSM parameters, with the exception of $A_0$, for which our projected limit appears somewhat weaker. We stress here that our method is generally applicable, and that the quantitative discrepancies observed with the ATLAS collaboration result are a consequence of the limited information available about the precise shape of the likelihood function. We therefore would urge experimentalists to make publicly available numerical fits to the likelihood functions that could be used to improved on the Gaussian assuption adopted here. We highlighted the computational advantage of our method which employs an effective likelihood at the mass spectrum level, which allows to shortcut the computationally expensive simulation of the whole experimental setup. We also demonstrated that, once LHC data become available, previously observed prior dependence of the results disappears if one adopts the broad, non-informative flat or log priors, although this may not be the case with any choice of this class of priors. We showed that the conclusions depend only mildly on which statistical quantity one chooses to adopt, i.e., Bayesian posterior or profile likelihood, in marked contrast with the present-day situation. The information from the likelihood can also be supplemented by a prior encoding a preference for "naturalness", thus suppressing the statistical weight of finely tuned regions. This choice leads to tighter errors on $m_0$ and $\tan\beta$, while hardly affecting the conclusions on $A_0$ and $m_{1/2}$. We then extended the analysis by adding to the likelihood function information about the neutralino dark matter relic abundance by imposing WMAP-like and Planck-like constraints. This improved the ability to reconstruct the value of especially $m_0$ and $\tan\beta$, much less so for $m_{1/2}$ (compared to the ATLAS data only case), while the bi-modality in the determination of $A_0$ could not be removed.

While the ATLAS SU3 point (and maybe also the CMSSM in the first place) may be unlikely to be realized in Nature, the method presented here appears to be powerful and robust enough to adequately reconstruct supersymmetric parameters from summary statistics of LHC measurements. The additional advantages presented here are the ability to easily investigate several different theoretical scenarios with relatively little computational effort, and the capability to produce predictions for derived observable quantities, such as for example the cosmological relic abundance and direct detection cross sections. The inclusion of observational constraints from such probes has also been demonstrated to be easily implemented. Finally, the favourable scalability of our MultiNest scanning algorithm with the dimensionality of the parameter space means that this method is in principle ready to investigate theories with several tens of free parameters, thereby opening the way to massive inference in supersymmetry phenomenology. As such we believe that our method will be a useful tool to face the real data that is expected to soon start arriving from the LHC, even if differs significantly from the case considered here.

**Acknowledgements**

The authors would like to thank D. Costanzo, R. Cousins, L. Lyons and D. Tovey for useful conversations, as well as C. Topfel and M. Weber for providing the covariance matrix used in the ATLAS Collaboration Report [9]. A communication with K. Desch, M. Uhlenbrock and P. Wienemann is also acknowledged. We would like to thank an anonymous referee for useful comments. L.R. is partially supported by STFC, the EC 6th Framework Programmes MRTN-CT-2004-503369 and MRTN-CT-2006-035505. The work of R.R. is supported in part by MEC (Spain) under grant FPA2007-60323, by Generalitat Valenciana under grant PROMETEO/2008/069 and by the Spanish Consolider-Ingenio 2010 Programme CPAN (CSD2007-00042). L.R. would like to thank the CERN Theory Division for hospitality during the final stages of the project. R.T. would like to thank the Galileo Galilei Institute for Theoretical Physics for the hospitality and the INFN and the EU FP6 Marie Curie Research and Training Network "UniverseNet" (MRTN-CT-2006-035863) for partial support.

# References

[1] G. L. Kane, C. F. Kolda, L. Roszkowski and J. D. Wells, *Phys. Rev.* **D49** (1994) 6173 [hep-ph/9312272].

[2] A. Chamseddine, R. Arnowitt and P. Nath, *Phys. Rev. Lett.* **49** (1982) 970;R. Barbieri, S. Ferrara and C. Savoy, *Phys. Lett.* **B119** (1982) 343;L. J. Hall, J. Lykken and S. Weinberg, *Phys. Rev.* **D27** (1983) 2359; for a review, see, e.g., H. P. Nilles, *Phys. Rept.* **110** (1984) 1.

[3] B. C. Allanach and C. G. Lester, *Phys. Rev.* **D73** (2006) 015013 [hep-ph/0507283]; B. C. Allanach, C. G. Lester and A. M. Weber, *JHEP* **0612** (2006) 065 [hep-ph/0609295]; B. C. Allanach, *Phys. Lett.* **B635** (2006) 123 [hep-ph/0601089].

[4] R. Ruiz de Austri, R. Trotta and L. Roszkowski, *JHEP* **0605** (2006) 002 [hep-ph/0602028]; L. Roszkowski, R. Ruiz de Austri and R. Trotta, *JHEP* **0704** (2007) 084 [hep-ph/0611173] and *JHEP* **0707** (2007) 075 [arXiv:0705.2012].

[5] J. R. Ellis, et al., *JHEP* **0605** (2006) 005 [hep-ph/0602220].

[6] O. Buchmueller *et al.*, arXiv:0808.4128 [hep-ph].

[7] N. Arkani-Hamed, et al., *JHEP* **0608** (2006) 070 [arXiv:hep-ph/0512190].

[8] I. Hinchliffe, et al., *Phys. Rev.* **D55** (1997) 5520 [hep-ph/9610544]; C. G. Lester and D. J. Summers, *Phys. Lett.* **B463** (1999) 99 [hep-ph/9906349]; W. S. Cho, et al., *Phys. Rev. Lett.* **100** (2008) 171801 [arXiv:0709.0288]; G. G. Ross and M. Serna, *Phys. Lett.* **B665** (2008) 212 [arXiv:0712.0943]; M. M. Nojiri, et al., *JHEP* **0805** (2008) 014 [arXiv:0712.2718]; H. C. Cheng, et al., *JHEP* **0712** (2007) 076 [arXiv:0707.0030].

[9] G. Aad, et al., [The ATLAS Collaboration], arXiv:0901.0512.

[10] B. C. Allanach, *Comp. Phys. Comm.* **143** (2002) 305 [hep-ph/0104145].

[11] G. Belanger, et al., *Comp. Phys. Comm.* **149** (2002) 103 [hep-ph/0112278]; *MicrOMEGAs: Version 1.3, Comput. Phys. Commun.* **174**, 577 (2006) [hep-ph/0405253].

[12] J. Dunkley et al. [The WMAP Collaboration], *Astrophys. J. Suppl.* **180** (2009) 306 [arXiv:0803.0586].

[13] M. M. Nojiri,et al., *JHEP* **0603** (2006) 063 [hep-ph/0512204].

[14] The Planck Collaboration, astro-ph/0604069.

[15] B. C. Allanach, et al., G. Belanger, F. Boudjema, A. Pukhov and W. Porod, hep-ph/0402161.

[16] F. Feroz and M. P. Hobson *Mon. Not. Roy. Astron. Soc.* **384** (2008) 449; F. Feroz, et al., arXiv:0809.3437.

[17] B. C. Allanach, et al., *JHEP* **08** (2007) 023 [arXiv:0705.0487].

[18] R. Trotta, et al., *JHEP* **0812** (2008) 024 [arXiv:0809.3792].

[19] Y. Akrami, et al., JHEP **1004** (2010) 057 [arXiv:0910.3950 [hep-ph]].

[20] M. E. Cabrera, J. A. Casas and R. R. de Austri, *JHEP* **0903** (2009) 075 [arXiv:0812.0536].

[21] M. E. Cabrera, A. Casas and R. R. de Austri, JHEP **1005** (2010) 043 [arXiv:0911.4686 [hep-ph]].

[22] J. R. Ellis, K. Enqvist, D. V. Nanopoulos and F. Zwirner, Mod. Phys. Lett. A **1** (1986) 57.

[23] R. Barbieri and G. F. Giudice, Nucl. Phys. B **306** (1988) 63.

[24] See: `http://www.superbayes.org/`

[25] E. A. Baltz, et al., *Phys. Rev.* **D74** (2006) 103521 [hep-ph/0602187].

[26] K. L. Chan, U. Chattopadhyay and P. Nath, *Naturalness, weak scale supersymmetry and the prospect for the observation of supersymmetry at the Tevatron and at the LHC*, *Phys. Rev.* **D58** (1998) 096004 [hep-ph9710473 ].

[27] J. L. Feng, K. T. Matchev and T. Moroi, *Multi - TeV scalars are natural in minimal supergravity*, *Phys. Rev. Lett.* **84** (2000) 2322 [hep-ph9908309 ] and *Focus points and naturalness in supersymmetry*, *Phys. Rev.* **D61** (2000) 075005 [hep-ph9909334 ].